# D.1.2.1 – Report describing surveys methodology



All PPs

## Document Control Sheet

| | |
|---|---|
| **Project number:** | ITHR0200175 |
| **Project acronym** | RESONANCE |
| **Project Title** | impRoving landslidE riSk preventiOn aNd mAnagement iN Coastal arEas |
| **Start of the project** | March 2024 |
| **Duration** | 30 months |

| | |
|---|---|
| **Project activity** | 1.2 Integrated survey/monitoring system |
| **Deliverable number & name** | 1.2.1 Report describing surveys methodology |
| **Type of deliverable** | Report |
| **Language** | English |
| **Work Package Number and Title** | WP1 |
| **Work Package Leader** | PP2-CNR |

| | |
|---|---|
| **Status** | Final |
| **Author(s)** | Mirko Francioni, Paolo Stocchi, Stefano Morelli, Simone Galeotti, Giulio Pappafico, Mariagiulia Annibali Corona – **LP-UNIURB**; Giovanni Leucci, Lara De Giorgi, Giuseppe Cavuoto, Daniela Tarallo, Michele Punzo, Maurizio Lazzari, Ivan Ferrari, Vincenzo Di Fiore, Francesco Giuri – **PP2-CNR**; Igor Ružić, Josip Peranić, Martina Vivoda Prodan, Željko Arbanas, Matea Zupičić – **PP3-GRADRI**; Filippo Invernizzi - **PP4-CRP**; Ivan Pentek, Vedrana Špada, Ener Špada – **PP5-IV** |
| **Version** | 1 |
| **Due date of deliverable** | 31/08/2025 |
| **Delivery date** | 30/08/2025 |

# INDEX

# 1. INTRODUCTION

In this report all the PPs contribute to describe the survey's methodologies used for the study of the four case studies. The goal is to present a guideline for geomechanical, geophysical and remote sensing (UAV and handle laser scanning) surveys in coastal areas that could be used in future by other operators. In the report the PPs have reported both technical information about these techniques and suggestions that could help during future survey's campaigns for obtaining more accurate data.
The report is structure as follow:

1. Geomechanical surveys and data analysis
2. Geophisycal survey and data analysis
3. Drone survey and data analysis
4. Handle LiDAR survey and data analysis

# 2. GEOMECHANICAL SURVEY AND DATA ANALYSIS

A rigorous geomechanical analysis begins with a comprehensive site description, including general characteristics, geological context, volumes of already mobilized blocks, rock mass typology, degree of weathering, and a detailed assessment of the fracture state through the quantification of discontinuities. Following an initial visual inspection of the outcrop, aimed at identifying the key geological and structural features, the first operational step is the establishment of a scanline survey. This involves laying a measuring tape or line taut across the surface of the rock mass, assuming the surface can be approximated as planar.

The orientation of both the rock face (dip and strike) and the scanline (trend and plunge) must be accurately measured to correctly contextualize all subsequent data within the structural framework. Moreover, for a proper analysis of the slope discontinuities, at least two scanline surveys should be carried out, each oriented orthogonally to the other.

## 2.1. Discontinuity Characterization and Data Collection

For each discontinuity intersecting the scanline, the following key geomechanical parameters are recorded, in accordance with the guidelines of the International Society for Rock Mechanics (ISRM, 1978):

a) Rock type: type of rock visible in outcrop (A in fig. 1).
b) Orientation: Strike and dip (or dip direction and angle) of the discontinuity (E in fig. 1).
c) Distance: The location along the scanline where the discontinuity intersects the line, noted as a progressive measurement.
d) Censoring: Evaluation of the visible portion of the discontinuity, using trimming and curtailment parameters to estimate the actual trace length across the scanline.
e) Spacing: The perpendicular distance between discontinuities of the same set, critical for calculating the Volumetric Joint Count (VJC) and defining the Volume of Rock Units (VRU), which represent the dimensions of potentially detachable blocks. Smaller spacing generally indicates smaller block sizes (I in fig. 1).
f) Origin: Classification of the genetic nature of the discontinuity, e.g., joints, bedding planes, faults, or other structural breaks (D in fig. 1).
g) Length: The visible trace length of the discontinuity on the outcrop, categorized as follows:
    - Very short: < 1 m
    - Short: 1–3 m
    - Medium: 3–10 m
    - Long: 10–20 m
    - Very long: > 20 m
h) Persistence: Continuity of the discontinuity across the rock face, indicating whether it (J in fig. 1):
    - Terminates against the rock matrix,
    - Terminates against another discontinuity,
    - Extends beyond the visible rock face (not observable).
i) Aperture: Perpendicular distance between the two surfaces of the discontinuity, indicating its degree of opening or closure (G in fig. 1). Aperture classes include:
    - Closed:
        - Tight (< 0.1 mm);
        - Slightly open (0.1–0.25 mm).

- Open:
    - Partially open (0.25–0.5 mm);
    - Open (0.5–2.5 mm);
    - Very open (2.5–10 mm).
- Wide:
    - Wide (10–100 mm);
    - Very wide (> 100 mm).

m) Roughness: Surface irregularity and deviation from a mean plane, assessed visually or measured using a profilometer (F in fig. 1).

n) Large-Scale Morphology: Macroscopic form of the discontinuity, distinguished as planar, undulating, or segmented.

o) Infill Material: Presence of material within the discontinuity (H in fig. 1):
- Absent
- Present and compact (e.g., sealed gouge)
- Present and incoherent (e.g., soft or friable material)

p) l) Water Presence (M in fig. 1).: Visual evidence of water within or seeping through the discontinuity.m) Surface Strength (B in fig. 1).: Uniaxial compressive resistance of the discontinuity surfaces, determined using an L-type Schmidt hammer to derive the rebound index (R) and the Joint Compressive Strength (JCS).

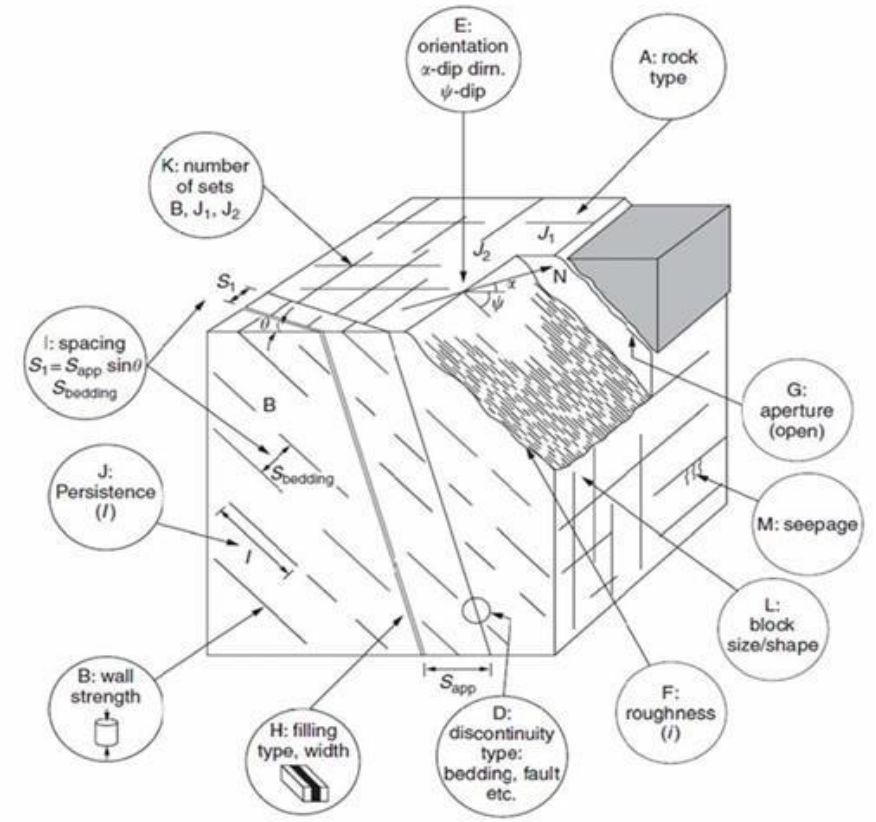


Figure 1 – Diagram illustrating rock mass properties (Wyllie, 1999).

## 2.2. Representation and interpretation of field data

Once the field data acquisition phase is completed, the next essential step involves the accurate and detailed representation of the collected geomechanical data. This process plays a critical role in enabling the structural interpretation of the rock mass, as it allows for the identification of dominant patterns discontinuity families, and potential kinematic scenarios of instability.

To this end, a series of graphical representations and statistical tools are employed, each designed to emphasize specific geometrical or spatial characteristics of the discontinuities. The following methods are among the most adopted for data analysis and visualization:

### 2.2.1. Pole Density Diagram

This stereographic representation projects all measured discontinuity orientations from a given survey station onto the lower hemisphere of a stereonet, where each plane is represented by its corresponding pole. The resulting diagram visually illustrates the density of pole concentrations, allowing the analyst to identify prevailing structural trends and the spatial

clustering of discontinuities. By applying contouring techniques, it becomes possible to highlight areas of higher pole concentration, which correspond to dominant discontinuity sets. Distinct symbols and colors are often used to differentiate between various types of structural features (e.g., bedding planes, joints, shear zones), facilitating a more nuanced structural interpretation.

### 2.2.2. Rose Diagram

This circular histogram is used to represent the azimuthal distribution of the discontinuities. Each segment or "petal" of the diagram corresponds to a directional interval, and its length is proportional to the number of discontinuities falling within that range. The rose diagram provides an intuitive visual summary of the preferential orientations within the dataset, making it particularly useful for quickly recognizing the dominant directionality of discontinuity families across the survey area.

### 2.2.3. Bar Histograms

Bar charts are constructed to statistically describe the geometric characteristics of the discontinuities. These typically include:
Length: measured in meters, indicating the visible extension of each discontinuity.
Aperture: expressed in millimeters, representing the perpendicular opening between the surfaces of the discontinuity.
Roughness: categorized into standardized roughness profiles (e.g., Barton profiles), allowing the comparison of surface textures.
By plotting these attributes separately, the histograms provide a clear and concise view of the distribution patterns within each parameter class, enabling the detection of dominant ranges or outliers. To synthesize and interpret the full set of field data, more advanced analytical methods are applied. These tools help summarize complex datasets and extract meaningful patterns.

### 2.2.4. Clustering Analysis

This technique involves projecting all recorded discontinuity poles onto an equal-area stereographic net (typically a Schmidt net), which ensures uniform angular representation. Discontinuities are grouped based on spatial proximity and orientation similarity, resulting in the identification of discontinuity sets (clusters). Each cluster is assigned a unique symbol or colour, and its representative mean plane is determined and visualized using great-circle arcs (also known as cyclographic traces). This allows for the precise characterization of each set's average orientation and structural relevance within the rock mass.

### 2.2.5. Summary Tables

To complement the graphical outputs, structured summary tables are compiled for each geomechanical survey station. These tables include the following key elements:

- Station identification and geographic location;
- Orientation of the rock face (strike and dip);
- Discontinuity sets derived from the clustering analysis;
- Representative poles and mean orientations for each set;

- Statistical dispersion indices (e.g., Fisher's K parameter), which quantify the angular variability of discontinuities within each family.

These summaries provide a concise yet comprehensive overview of the structural framework encountered at each station, facilitating comparisons across different parts of the site.

#### 2.2.6. Composite Stereographic Projection

This is a holistic visualization that combines the primary discontinuity sets and the orientation of the rock face into a single equal-area stereographic projection. The great-circle traces of each set are plotted together with the orientation vector of the outcrop face (often labeled as F), providing a synthetic overview of the structural setting. This diagram is particularly valuable for performing kinematic analyses, as it allows for a visual evaluation of the geometric compatibility between discontinuity orientations and potential failure mechanisms (e.g., planar sliding, wedge failure, toppling).

## 2.3. Geomechanical parameters of the rock mass

To complete the geomechanical analysis of a rock mass, it is necessary to determine several key parameters that quantify both the quality and the intensity of fracturing. The most assessed indices include: a) RQD (Rock Quality Designation), b) Jv (Joint Volumetric Count), d) Vb (Block Volume); These parameters are calculated based on field survey data, typically obtained through geomechanical mapping, photogrammetry, laser scanning of slopes, and other high-resolution surveying methods and form an integral part of the site's geomechanical characterization.

### 2.3.1. Rock Quality Designation

The RQD index, developed by Deere et al. in 1967, provides a quantitative estimate of rock mass quality based on core drilling results. It is defined as the ratio (expressed as a percentage) of the total length of intact core pieces longer than 10 cm (4 inches) to the total length of the core run. To ensure reliable results, drilling should be carried out using at least NW-type core barrels, in accordance with ISRM recommendations. This includes a minimum core diameter of 54.7 mm (2.15 inches), double-tube core barrels, diamond bits, and a slow drilling advance rate. Proper fragment measurement and calculation procedures for RQD are illustrated in Figure 2. Based on the calculated RQD value, the quality of the rock mass can be classified into five main categories:

a) Very poor: 0%–25%
b) Poor: 25%–50%
c) Fair: 50%–75%
d) Good: 75%–95%
e) Excellent: 95%–100%

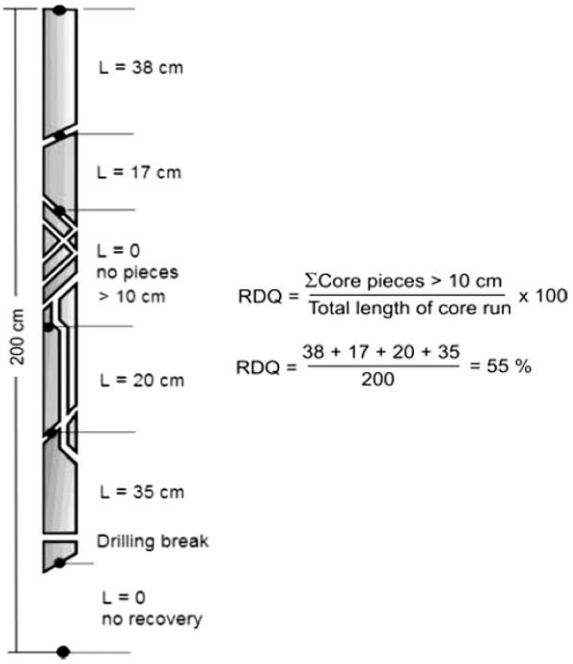


Figure 2 – Procedure for the measurement and calculation of RQD (Deere, 1989).

### 2.3.2. Volumetric joint count (Jv)

The Volumetric Joint Count (Jv) was first introduced and described by Palmstrøm (1982, 1985) and later expanded upon by Sen and Eissa (1991, 1992). This parameter quantifies the degree of fracturing in a rock mass based on the representative spacing, typically the median spacing of each identified discontinuity set. As such, the determination of Jv requires a preliminary clustering analysis to group discontinuities into statistically significant families. Once the main joint sets have been identified, the volumetric joint count is calculated using the following equation:

$$J_v = \frac{1}{S_1} + \frac{1}{S_2} + \frac{1}{S_3}$$

Where:

- $S_1$, $S_2$, $S_3$ are the average or median spacings (in meters) of the principal discontinuity sets within the rock volume under analysis.

In addition to systematic joints, random or non-persistent discontinuities may also be accounted for in the volumetric joint count. In such cases, a conventional spacing value is

assigned to each random discontinuity, typically assumed to be Sr= 5 meters, based on empirical observations and field experience. This leads to an extended form of the equation:

$$J_v = \frac{1}{S_1} + \frac{1}{S_2} + \frac{1}{S_3} + \cdots + \frac{N_r}{5}$$

Where:

- $N_r$ represents the number of observed random discontinuities within the investigated rock mass volume.

In situations where core drilling is not feasible or practical, Palmstrøm (1982) proposed an empirical correlation that enables the estimation of the Rock Quality Designation (RQD) based on the volumetric joint count (Jv). This correlation is particularly applicable to non-clayey rock masses, and is expressed by the following equation:

$$RQD = 115 - 3.3 \times J_V$$

In this context, the volumetric joint number (Jv) is equivalent to the sum of the joint frequencies (expressed in joints per meter) associated with the various discontinuity sets identified in the rock mass. By calculating both the Jv and the corresponding RQD value, it is possible to determine the fracture class of the rock mass under investigation. This classification can then be used to assign the rock mass to one of the predefined fracture intensity categories, as outlined in Table 1.

Table 1 – Fracture Classes of the Rock Mass Based on Jv and RQD.

| FRACTURING CLASS | Jv | RQD |
|---|---|---|
| Massive | < 0.3 | Excellent (4.5 < Jv < 7.6) |
| Very slightly fractured | 0.3 - 1.0 | |
| Slightly fractured | 1.0 - 3.0 | |
| Moderately fractured | 3.0 – 10.0 | Good (7.6 < Jv ≤ 12.1) |
| Highly fractured | 10.0 – 30.0 | Fair (12.1 < Jv ≤ 19.7) |
| | | Poor (19.7 < Jv ≤ 27.3) |
| Very highly fractured | 30.0 – 100 | Very Poor (Jv > 27.3) |
| Crushed | >100 | |

Given the high sensitivity of the Rock Quality Designation (RQD) to the orientation of the borehole, since the core may intersect discontinuities differently depending on the drilling direction, estimating RQD through the volumetric joint count (Jv) offers a valid alternative approach for assessing rock mass quality. This method significantly reduces the directional variability inherent in direct core-based measurements.

Moreover, when using core samples for RQD determination, it is essential to differentiate between natural fractures and those induced by drilling tools or core handling. Similarly, in the case of surface exposures or underground excavations, blast-induced or excavation-related fractures must be excluded from the analysis to ensure the accuracy of the rock mass quality estimate.

In the absence of core drilling, the RQD index can also be indirectly estimated from discontinuity surveys conducted along a scanline (linear survey) or over a scan area (surface mapping). This is done by applying the empirical relationship proposed by Palmstrøm (1982) to the weighted joint density (wJd) (Fig. 3). In this alternative approach, there is no need for clustering analysis or for the identification of distinct discontinuity sets, as the calculation is based on the total number of discontinuities recorded, regardless of their orientation.

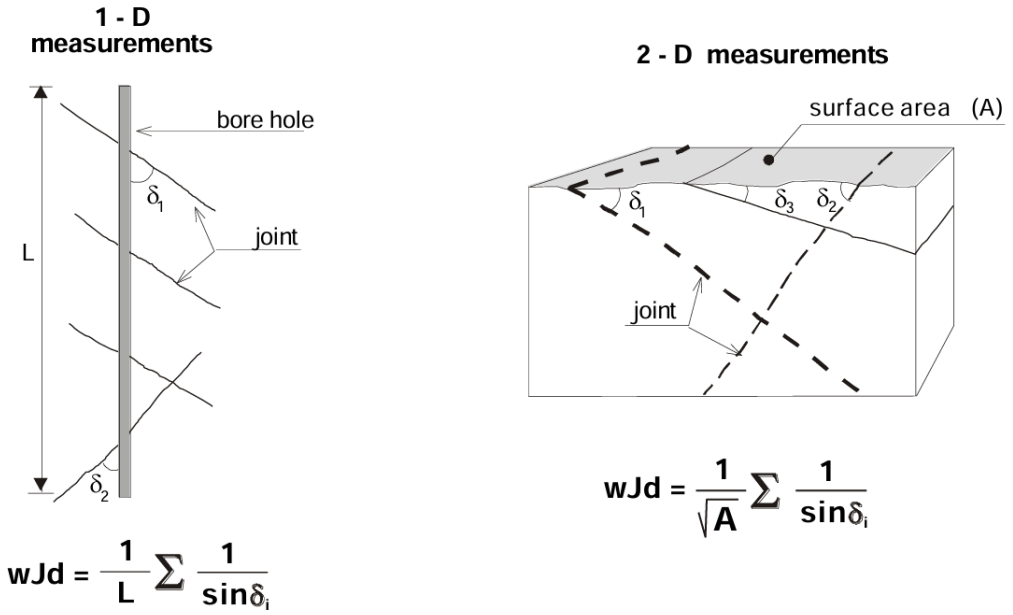


Figure 3 – Intersection Between Discontinuities and a Borehole (left), and Between Discontinuities and a Surface (right) (from Palmström, 1995).

According to Palmström (2001), the parameters of a rock mass that most significantly influence its mechanical behavior and strength characteristics can be grouped into the following main categories:

- Degree of Fracturing, which includes:
  - Discontinuity density, typically quantified through the spacing of fracture sets, block size, and Rock Quality Designation (RQD).
  - Block shape or the overall fracture pattern;
  - Orientation of the principal fracture sets or dominant discontinuities.
  - Discontinuity Characteristics, including:
  - Surface roughness of the discontinuities, encompassing smoothness, waviness, or planarity.
  - Surface condition or alteration, referring to the state of the discontinuity walls and the presence of infilling materials, such as clay or mineral deposits.

- Properties of the Intact Rock Material between discontinuities, comprising:
  - Strength and elastic properties of the rock matrix;
  - Rock anisotropy, in terms of directional variability in mechanical behavior;
  - Rock durability, or the capacity of the material to maintain integrity over time under environmental or mechanical stressors;
  - Presence of minerals with specific behaviours, such as swelling, elastic deformation, or solubility.

The scale of the rock mass under investigation is generally so large that it is, in most cases, impossible to directly measure its mechanical properties. Therefore, the most effective way to obtain information regarding the discontinuity properties (density and other fracture characteristics) within the rock mass is through field observations or borehole core analysis. The methodology employed in these observations strongly influences the quality of the geomechanical data used for evaluations and calculations.

The discontinuity spacing within a system is defined as the distance between individual fractures belonging to that same system. When multiple discontinuity systems are present, the average spacing is not calculated as a simple arithmetic mean but rather using the inverse summation formula:

$$\frac{1}{S_a} = \frac{1}{S_1} + \frac{1}{S_2} + \frac{1}{S_3} + \cdots$$

where $S_a$ is the average spacing, and $S_1$, $S_2$, $S_3$ represent the spacings of the individual systems.

In the case of borehole core data, the average length of core fragments intercepted by joints (joint intercept length) often does not correspond to the true spacing of a given discontinuity system, as it may include joints from multiple systems as well as random fractures.

The term “discontinuity spacing” is frequently ambiguous and can lead to confusion or misinterpretation, as it is not always clearly defined with respect to the specific measurement technique or fracture system being referenced.

In the context of slope stability analysis in rock or underground excavations, it is crucial to define block size, which in turn is controlled by the number of discontinuity sets, their orientation, and spacing.

According to Dearman (1991), when a relatively regular fracture system is present, the discontinuity network can be systematically described. However, Palmström (2001) clearly illustrated that in most real cases, fracture patterns rarely exhibit such regularity. Under these conditions, a simplified classification proves more practical, such as dividing blocks into four main categories, as illustrated in Figure 4.

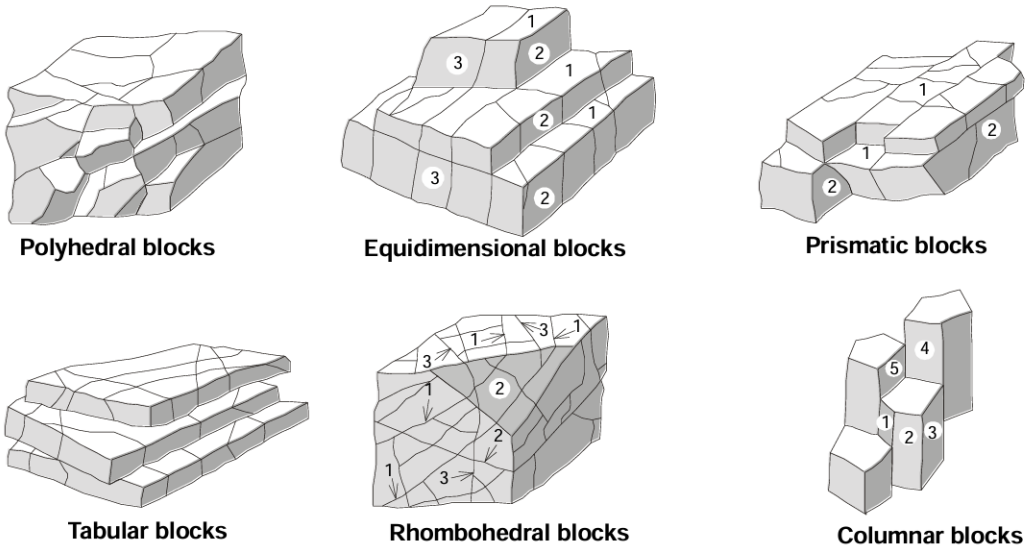


Figure 4 – Examples of Block Shapes or Discontinuity Patterns (Dearman, 1991).

### 2.3.3. Block Volume (Vb) Estimation

When rock blocks are visible in outcrop, their volume can be directly estimated by measuring the average dimensions of a representative sample. For small-sized blocks or fragments (on the order of cubic decimeters or smaller), this approach is particularly effective, as it allows

for a quicker assessment compared to the complete mapping of all discontinuities. In settings characterized by irregular fracturing, the detailed survey of every discontinuity is time-consuming and often inefficient. In such cases, direct measurement of block volume frequently represents a more practical and accurate alternative. Volume estimation can also be performed on borehole cores when the fragments are sufficiently small to be measured, such as in the case of intensely fractured or crushed rock.
When three discontinuity systems are present, the block volume Vb can be calculated as:

$$V_b = S_1 \cdot S_2 \cdot S_3 \cdot (sin\ sin\ \gamma_1\ \cdot sin\ \gamma_2 \cdot sin\ sin\ \gamma_3\ )$$

where:

- S1, S2, S3 are the spacings between the three discontinuity sets;
- γ1, γ2, γ3 are the angles between the respective discontinuity planes.

In cases where the three discontinuity systems intersect approximately at right angles, the formula simplifies to:

$$V_b = S_1 \cdot S_2 \cdot S_3$$

However, it is often not possible to observe individual blocks in outcrop. In such instances, the spacing of random discontinuities may be assumed to be approximately 5 to 10 times the spacing of the main discontinuity set.

# 3. GEOPHISYCAL SURVEY AND DATA ANALYSIS

In the field of applied geophysics, geoelectric methods have been important for about a century, particularly for shallow and near-surface investigations. Geoelectric methods are used extensively to locate buried targets that are conductive and resistive in nature. The purpose of active geoelectric surveys is to determine the subsurface resistivity distribution by making measurements on the ground surface. The ground resistivity is related to various geologic parameters such as the mineral and fluid content, porosity, and degree of water saturation in the rock.

Geoelectric surveying has greatly improved and has become an important and useful tool in archaeological and monumental heritage conservation state studies and in hydrogeology, in environmental and engineering applications (e.g., Amidu & Olayinka, 2006; Aizebeokhai et al., 2010; Dahlin &Loke, 1997; Griffiths et al., 1990; Leucci, 2006; Leucci, 2007; Leucci et al., 2014; Negri et al., 2008; Leucci et al., 2017).

Schlumberger brothers introduce the resistivity method in the second decade of the twentieth century (Loke et al., 2013; Sarma, 2014). In the origin of this technique, the center point of the electrode array remains fixed, but the spacing between the electrodes is increased to

obtain more information about the deeper sections of the subsurface. The traditional horizontal layering techniques for interpreting geoelectric resistivity data are rapidly being replaced with two-dimensional (2D) and three-dimensional (3D) models of interpretations, especially in complex and heterogeneous subsurface media. Field techniques have advanced from the measurements made at separate and independent points to automated measuring systems with multielectrode array along the measurement profiles.

## 2.1. About electrical resistivity method

The physical parameter in geoelectric measurements is the specific electric resistivity $\rho$ of the ground. The applications of 2D and 3D imaging are nowadays important for visualizing and interpreting complex archaeological structures at various depths (Negri et al., 2008). The electric resistance, $R$, of a material is related to its physical dimension, cross- sectional area, $S$, and length, $l$, through the electric resistivity, $\rho$, by Reynolds (Reynolds, 2011):

$$\rho = R \cdot \frac{S}{l}$$

Active resistivity method uses a dipole source of current injected into the subsurface through point electrodes, and the resulting potential difference is measured at other electrode positions in the neighborhood of the current flow (Fig. 5).

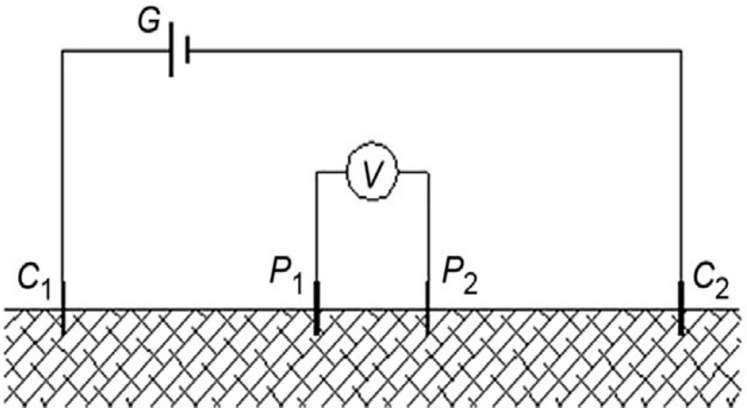


Figure 5 - Active resistivity method scheme.

Considering a completely homogeneous and isotropic medium for a semiinfinite conducting layer of uniform resistivity bounded by the ground surface, a current of strength I is injected at a point C1 into the ground surface. The current I will flow away radially from the point of source, and its distribution will be uniform over a hemispheric shell of an underground region (Fig. 6) of resistivity $\rho$.

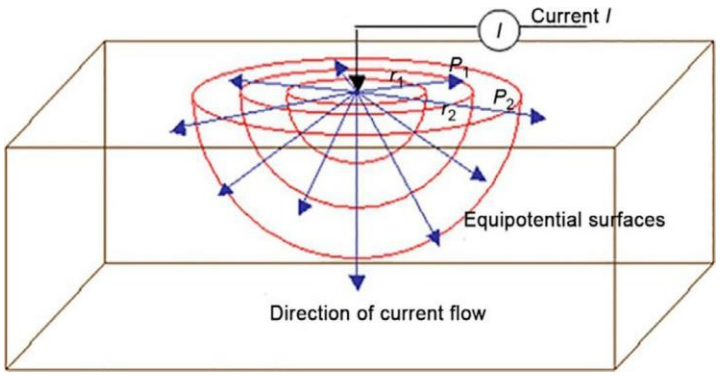


Figure 6 - Schematization of current flow from point source.

At a distance *r* of a point *P* in the medium from the point source, the surface area of the hemispheric shell is $2\pi r^2$ so that the potential for the homogeneous half-space is

$$V(r) = \left(\frac{\rho I}{2\pi r}\right) cos\ cos\ t$$

The potential function, considering the two points $P_1$ and $P_2$ at distance $r_1$ and $r_2$ from the point source (Fig. 9), is obtained by applying the before Eq.

$$V(r) = \frac{\rho I}{2\pi r}\left(\frac{1}{r_1} - \frac{1}{r_2}\right)$$

Thus, if the $P_1$ and $P_2$ are the potential electrodes and $C_1$ and $C_2$ are the current electrodes (Fig. 5), the potential difference between $P_1$ and $P_2$ can be written as

$$\Delta V = \frac{\rho I}{2\pi r}\left(\frac{1}{C_1P_1} - \frac{1}{C_1P_2} - \frac{1}{C_2P_1} + \frac{1}{C_2P_2}\right)$$

But subsurface isn't a homogeneous medium; it is typically heterogeneous. Therefore, the estimated electric resistivity must be considered as apparent electric resistivity $\rho_a$:

$$\rho_\alpha = K \cdot \left(\frac{dV}{I}\right)$$

$K$ is the geometric factor.

### 3.1.1. Electrical resistivity field data acquisition

The subsurface and the investigated medium are usually complex and multiscale, and spatial variation can change rapidly both laterally and vertically along survey pro- files, since survey design must take into account the capability of the system for data acquisition; the target (shape and dimensions); and therefore the required resolution, the medium heterogeneity, the areal extension the cost, and the time required to complete the survey. Generally, as shown in Figure 5, four electrodes are placed at arbitrary locations on the ground surface. Therefore, there are a number of electrode configurations that can be used in recording electric resistivity field data. Conventional arrays most used include Wenner (alpha), Schlumberger, dipole-dipole, pole-pole, and pole-dipole arrays (Fig. 7), each one suitable for a particular geologic situation. The array choice depends on a number of factors related to the target to be delineated, heterogeneities of the medium, sensitivity of the resistivity

meter system, the background noise level, electromagnetic coupling, sensitivity of the array to vertical and lateral resistivity variations, its depth of investigation, and the horizontal data coverage and signal strength of the array. The Wenner (alpha) and Schlumberger arrays are relatively sensitive to vertical variations in the resistivity below the centre of the array but less sensitive to horizontal variations in the subsurface, and it has a moderate depth of investigation. A limitation of this array is the relatively poor horizontal coverage with increased electrode spacing (Reynolds, 2011).

Dipole-dipole is very sensitive to horizontal variations of resistivity and relatively insensitive to vertical variations of resistivity in the investigated medium. Thus, it is the most preferred array for mapping vertical structures like walls, dykes, tombs, and cavities. It is the most sensitive array to 3D structure (Reynolds, 2011). The depth of investigation of the array depends on both the current electrode spacing a and the distance between the two dipoles n and is generally shallower than the Wenner array, but it has a better horizontal data coverage than Wenner array. It has a major disadvantage that consists in a decrease in signal strength with increasing distance between the dipole pair.

The pole-dipole array is an asymmetrical array; it has relatively good horizontal coverage and higher signal strength compared with dipole-dipole array. Repeating measurements with the electrodes arranged in the reverse order can eliminate the asymmetrical effect. The signal strength of the pole-dipole array is lower than that of Wenner and Schlumberger arrays and is very sensitive to vertical structures.

The pole-pole array consists of one current and one potential electrode with the second current and potential electrodes at infinite distances. Finding suitable loca- tions for these electrodes so as to satisfy this theoretical requirement is often difficult. It has the widest horizontal coverage and the deepest depth of investigation but the

poorest resolution. The resolution of the pole-pole array is very poor as subsurface structures tend to be smeared out in the inversion model (Reynolds, 2011).

Wenner alpha

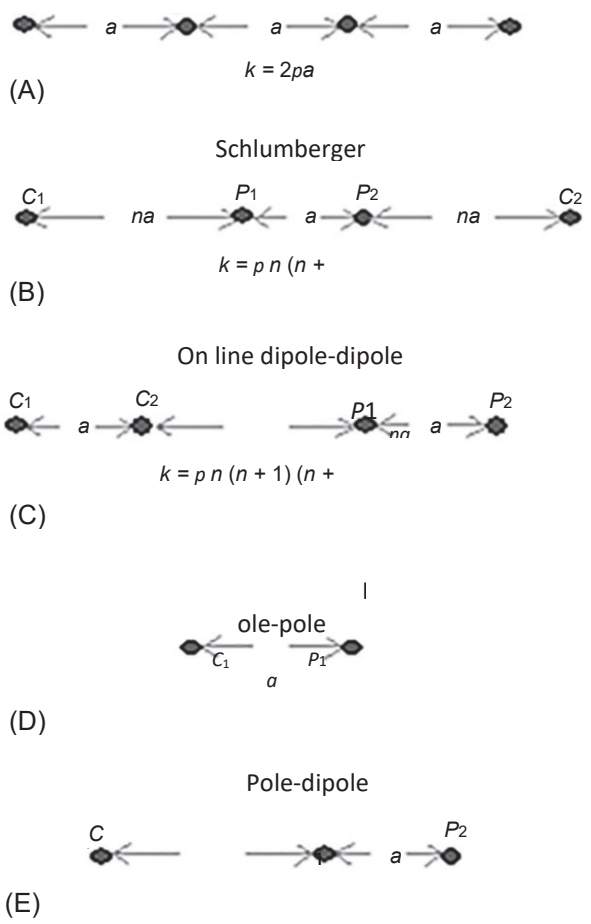


Figure 7 - The electrodes array commonly used in electric resistivity data acquisition. (A) Wenner alpha;(B) Schlumberger; (C) on line dipole-dipole; (D) pole-pole; (E) pole-dipole.

The apparent-resistivity values observed by the different array types over the same structure can be very different.

Resistivity field data are acquired using several types of earth resistivity meter. The equipment is portable, light weight, and relatively cost-effective when compared with other geophysical data acquisition systems. A conventional setup of the earth resistivity meter (Fig. 8) basically consists of the following: a constant current source, commonly a battery pack connected to a unit control composed of (i) a commutated DC circuit to change polarity of the current source, (ii) an ammeter that measures the injecting current, and (iii) a very sensitive voltmeter that measures the response signal. Furthermore, a computer with an acquisition software allows to see in real time the resistivity data. Electrode is usually

stainless steel. Two-dimensional (2D) resistivity imaging can be achieved by integrating the techniques of vertical electric sounding with that of electric profiling. They are usually carried out using large numbers of electrodes connected to multicore cables (Fig. 9). For a system with a limited number of electrodes, was developed a survey method in which the area covered by the survey can be extended along the survey line by moving the cables past one end of the line by several units of electrode spacing (roll-along method). The values of apparent resistivity observed are presented in pictorial form using pseudosection contouring that gives an approximate picture of the resistivity distribution in the measured medium. The shape of the con- tours depends on the type of array used in the investigation and the distribution of the true resistivity. Three-dimensional survey, in theory, gives the most accurate and reliable results especially in heterogeneous medium.

Figure 8 - The field electric resistivity data acquisition instrument.

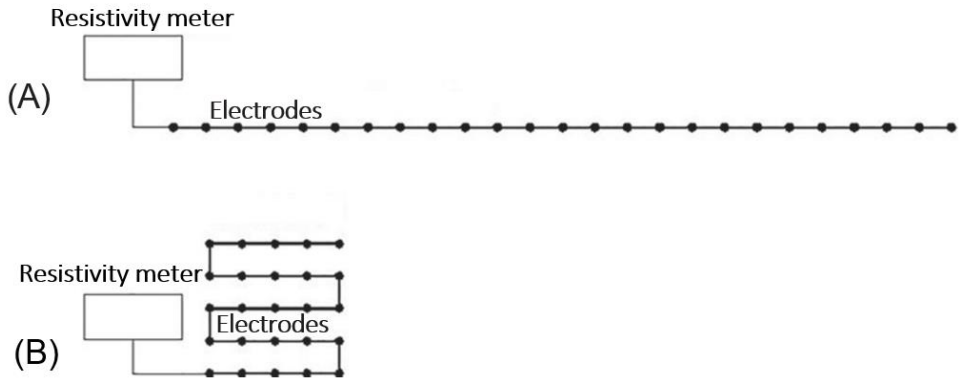


Figure 9 - The multielectrodes 2D (A) and 3D (B) acquisition scheme.

Ideally, the measurements of apparent-resistivity values that would constitute a complete 3D data set should be made in all possible directions.

In practice, instead of using the 3D measurement mode, 3D resistivity variations are recorded by recording a dense 2D measurement grid that is considered to be a more practical and economical approach for field data.

The 2D sets involve measuring parallel 2D lines with interline spacing equal to the interelectrode spacing and can take place along the *X* axis, *Y* axis, or along both axes. These 2D data are routinely interpreted with 2D algorithms, and the results are combined to generate pseudo 3D (*x*, *y*, and *z*) images. The obtained results are affected by artifacts due to the fact that 3D responses are related to 2D structures. Electric resistivity inversion method is related to the finite element method (FEM) in order to solve the forward problem. The technique has been extensively described in many works.

## 2.2. About seismic tomography

Tomography which has been used in science and technology as the object's internal-structure imaging technique is able to map the physical quantity distribution within the object non-destructively. It is an alternative way for quality inspection of many materials.

The basic idea of tomography imaging popped up when Radon presented a mathematical formula to reconstruct a 2-dimensional function of some integral function lines in two dimensional plane which then, is better known as Radon Transformation (for more see (Leucci, 2019; Leucci, 2020).

For sonic standard surveys, only the body waves P and S are considered. The travel time and the sonic pulse velocity provide basic information about the quality and conservation state of the medium element under investigation.

The sonic pulse-velocity test is very similar to the ultrasonic pulse-velocity test for what concerns basic theories, the purpose of the tests, and application of the method. The difference between the two methods regards the frequency of the emitted wave, as described previously.

The commonly used sonic methods are:

- sonic transmission method;
- sonic/seismic tomography;
- sonic/seismic reflection method;
- ultrasonic reflection method.

The sonic transmission method involves the propagation of a sonic wave through the thickness of the wall (or the structure) under investigation. Emission of the wave is performed on one side of the structure by the impact of the force hammer or pulsed generator; an accelerometer, positioned directly opposite the force hammer, receives the transmitted signal on the other side of the wall (Fig. 10a). The resulting wave velocity is an average of the local velocity along the path, and it is not possible to evaluate the position and the extent of any possible inhomogeneity. The velocity variations may be plotted on a contour map, with grid points as X and Y coordinates and the pulse velocity as the Z co-ordinate. This format makes possible a simple evaluation of the status of the masonry or concrete walls of the structure or an evaluation of the internal conditions of a structure. It has generally been recognized that the direct-transmission arrangement is a simple technique to apply in the analysis of structures since it provides a defined path length through the structure. Furthermore, since the arrival time of the first wave is of primary concern, no attempt to distinguish complex wave frequencies and reflections is required for the analysis. This method has been successfully used to evaluate material uniformity, detect the presence of voids, estimate the depth of surface crack, and calculate an average compressive strength for the structure or the material. The detection of flaws is possible due to the fact that sonic waves cannot transmit across an air gap, which could be due to a crack, void, or delamination at the interface between brick or stone and mortar. A propagating wave must find a path around the void, resulting in attenuation and an increase in the transit time of the signal. Figures 10b and c illustrate indirect transmission modes used mainly for tomographic surveys.

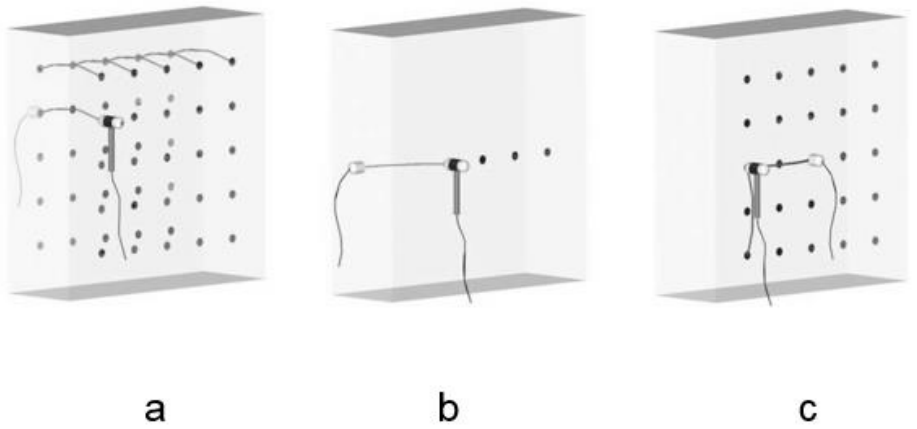


Figure 10 - Transmission modes for sonic wave tests: (a) direct; (b) semidirect; (c) indirect

Sonic tomography represents an improvement in the sonic-transmission test method because tests are performed not only in the direct mode but also along paths that are not perpendicular to the wall surfaces. The wall of the structure or the masonry section is thus traversed by a dense network of ray-paths, each of them defining a specific travel time between the sonic source and receiver. These values of travel time are processed in order to achieve a 3D reconstruction of the velocity distribution across the structure or selected cross-section; in this way, local variations of the velocity can be identified and correlated to zones of weakness or flaws in the internal fabric of the structure (Fig. 11).

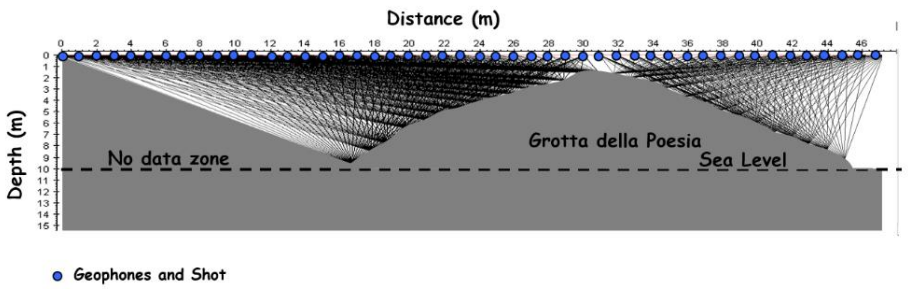


Figure 11 - Typical ray path in a tomography acquisition

It is usual to assume a homogeneous structural response in the application of the tomographic method. This is because the response is measured by transducers far from the

location of the impact, where inhomogeneous behavior may arise. Therefore, any variation from the expected travel time is attributed to inhomogeneity in the structure or damage has occurred. To increase the accuracy of the measurements, it is necessary to maximize the amount of experimental data included in any calculation used by ensuring that all areas of the proposed tomographic section have adequate ray-path coverage. A number of inversion algorithms are available commercially for tomographic reconstruction (Leucci, 2019; Leucci, 2020).

In the sonic reflection method, the emitters and receivers are on the same side of the masonry; thus, the stress wave recorded is the direct stress wave reflected from any internal flaw or the rear face of the structure being investigated. The value of velocity calculated from the rear wall or face of a structure or on the ground surface is a measure of the local velocities along the path. Seismic resolution is a measure of how large an object need to be to be seen by seismic methods. The vertical resolution is derived from the length of the soundwave, and layers can be discerned when their thickness is below ¼ wavelength. Still, it is possible to detect layers down to 1/32 wavelength. When referring to vertical resolution, it is normally at 1/4 wavelength. The wavelength is calculated by (Reynolds 2011):

$$\lambda = V/F$$

The vertical seismic resolution is calculated by λ/4, where λ is the wavelength, F is the seismic frequency, and V is the seismic velocity.

The seismic wave is sent out from the source move in 3D and spreads out over a larger area the further away it gets from the source. The horizontal resolution is derived from the Fresnel zone, the part of a reflector covered by the seismic signal at a certain depth. On a buried horizon, all features with a lateral extent exceeding the Fresnel zone will be visible. The radius of this zone is often taken as the horizontal resolution for unmigrated seismic data. As with the wavelength, the Fresnel-zone size also increases rapidly with depth (Leucci, 2019).

$$Fresnel\ zone = V \cdot (D/F)^{0.5}$$

Where:

- F is the seismic frequency, V is the seismic velocity, and D is the depth in time.

Sonic (S) and ultrasonic (US) can be used on built heritage with direct tomography (DT), semi-direct tomography (ST), indirect tomography (IT) transmission method, or with tomographic (T) mode, depending on the objective of the investigation. Problems that can be analyzed are listed in Table 2, with an indication of the most appropriate acquisition mode.

Table 2 - Target of sonic measurements.

| Target | Acquisition type |
|---|---|
| Detection of inhomogeneities (e.g., variation of material texture, repair interventions, presence of different materials...) | DT, T |
| Detection of multiple leaves and measurement of the thickness of each leaf | T |
| Detection of detached external leaves | DT, T |
| Detection of voids or chimney flues | DT, T |
| Evaluation of effectiveness of repair interventions (e.g., grout injections, repointing, etc.…) | DT, T, ST |
| Detection of damaged portions of structure or of crack patterns | DT, IT, T |

The successful application S methods depend on the appropriate application of the method, but there also exist unfavorable conditions where the application to some of these problems might fail. Sonic pulses do not undergo significant signal attenuation. The execution of the tests is thus generally successful. On the other hand, these methods are characterized by low resolution, which cannot be sufficient for the detection of small voids or small inclusions or when dealing with the detection of multiple leaves, detached external leaves, cracks, etc. Higher frequencies and smaller wavelengths are needed to improve the resolution, and this entails the use of US waves. The resolution of S tomographies depends also on the dimension of the grid used to transmit/acquire the sonic waves. However, very dense grids, if not accompanied using higher-frequency stress waves, may not lead to improved resolution. As the presence of moisture produces an apparent S and US pulse-velocity increase, the application of the method to very moist masonry should be carefully evaluated. If metal

elements (ties or anchorages) exist within the investigated structure, it is possible to observe an apparent S pulse-velocity increase. This is due to the faster propagation of the wave through the metal element; thus, the tests should be carried out at a certain distance from the position where the ties are placed. Care is needed when the hammer/accelerometer must be used on a precious surface decorated with frescos or plasters; in these cases, a good practice consists of protecting the surface (when hitting/receiving) from contact with a simple piece of clean paper. Table 3 shows some values of Vp and Vs for a wide variety of materials (Leucci, 2019).

Table 3 - P and S wave velocities in various types of geological materials.

| Material | Vp (m/s) | Vs (m/s) |
|---|---|---|
| Air | 330 | - |
| Dry sands | 400–1200 | 100–500 |
| Saturated sands | 1500–4000 | 400–1200 |
| Clay | 1,100–2,500 | 200–800 |
| Marne | 2,000–3000 | 750–1500 |
| Arenarie | 3000–4500 | 1200–2800 |
| Limestone | 3500–6000 | 2000–3000 |
| gypsum | 2300–2600 | 1100–1300 |
| Shale | 4500–5500 | 2000–3100 |
| dolomite | 3500-6500 | 1900–3600 |
| water | 1450 | - |
| Granite | 4500–6000 | 2500–3300 |
| Basalt | 5000–6,000 | 2800–3400 |
| Coal | 2200–2700 | 1000–1400 |
| Ice | 3400–3800 | 1000–1900 |

# 4. DRONE SURVEY AND DATA ANALYSIS

Drones are becoming a must-have tool for monitoring and survey buildings and all types of terrain, from flat areas to steep slopes, especially in the slopes they become fundamental to collect information in dangerous areas.

For the geologist that aims to study every type of terrain it is a tool that provides a variety of information that would otherwise be difficult to find. Starting from the photogrammetric survey to build a 3D model up to the LIDAR survey which allows to have a detailed DTM of the area. The last tool is the thermal camera, to be used if the Area of Interest has some exposed area without vegetation.

The purpose of this guide is to provide a primer for drone surveys, starting from how to get certified, the steps needed to plan a survey, what to do during the survey, and how to manage the data.

The first chapters (Certification, Limitations) are taken almost entirely from the EASA website (https://www.easa.europa.eu/en/light) and from the ENAC website (https://www.enac.gov.it/en/), two valuable aids for those who want to know more about drone regulation.

## 4.1. Certification

In order to conduct a Drone Survey it's necessary to obtain a certificate, the certificate is specific for every drone weight category. As reported in the Figure below, there are three drones weight categories. There are two certifications: one for the category A1/A3, one for the category A2. To conduct a geological survey is necessary only to have the certificate A1/A3 since it's expected to fly the drone in an area without people. A summary diagram is shown in the Figure 12.

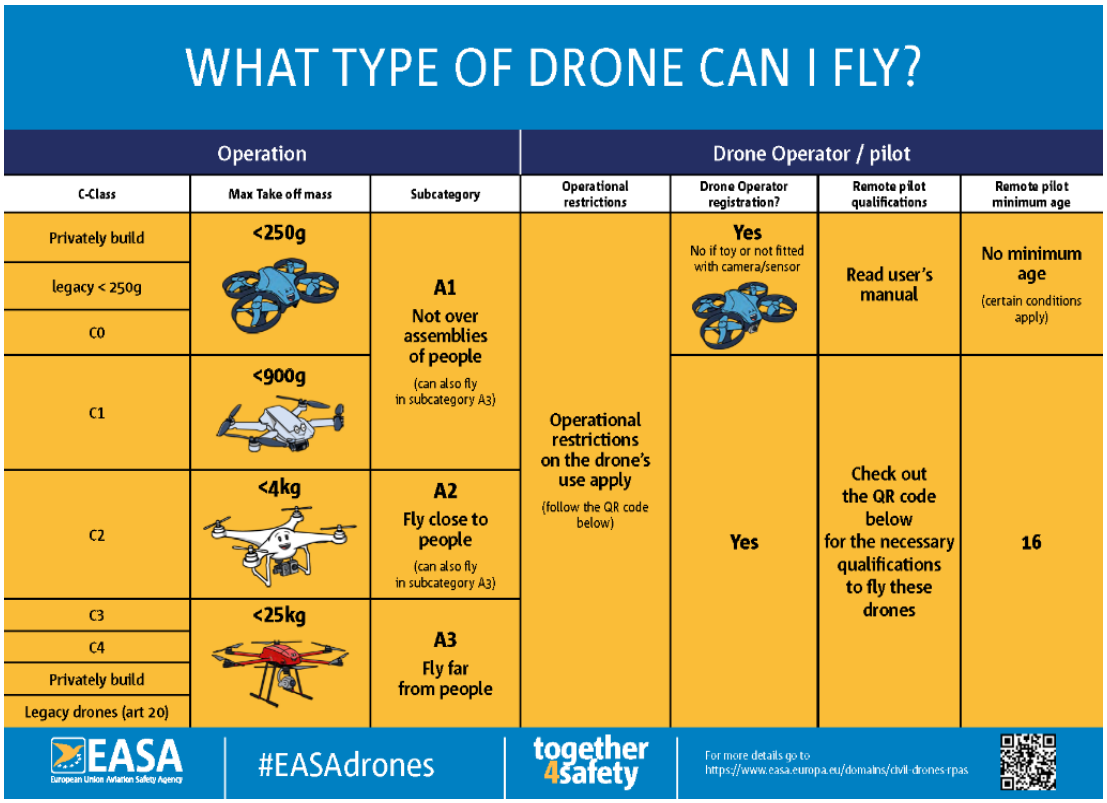


Figure 12 – Drone wights and necessary patents.

For the category A1/A3 requires an online exam. To become a UAS pilot in the OPEN A2 subcategory, it is necessary to obtain the "Remote Pilot Competence Certificate". It is issued upon satisfaction of three fundamental requirements:

- already having the "Online training completion test" for the A1/A3 categories;
- declare the completion of the practical training (Self-practical Training), carried out according to the conditions set for the OPEN A3 category and as specified in point UAS.OPEN.040 of EU Regulation 2020/639.

Implementing Regulation (EU) 2019/947 defines the methods by which the skills to pilot a UAS in the Open and Specific operation categories can be acquired.

According to Regulation (EU) 2019/947, all UAS remote pilot certificates issued after 31 December 2020 by one of the national authorities subject to EASA regulation are automatically recognised as valid by all other national authorities. For this reason, a remote

pilot in possession of an EASA certificate can operate freely within each EASA member state, in compliance with European legislation and in compliance with any additional national restrictions.

## 4.2. Limitations

Before flying a drone, please remember that the UAS operator is required to:

- have the drone flown by a pilot with adequate skills (ref. UAS Pilots page);
- successfully complete registration on the d-flight portal and acquire your European identification code, in QR code format, to be placed on each of the UAS (drones) you operate with (ref. Drone Operators (UAS) page);
- have taken out adequate insurance from the UAS operator;
- check what is required for carrying out operations in the open category – open category or in the specific category – specific category;
- check the compatibility of the airspace in which you intend to operate with the type of operations chosen.

### 4.2.1. Drone (UAS) geographical zones

To keep aircraft and people on the ground safe, drone geographical zones, or geo-zones, have been set up across Europe by the different States. Geo-zones are portions of airspace where drones, or to use the more official term Unmanned Aerial System (UAS), operations are facilitated, restricted or excluded.

The geo-zones are available on the portal d-flight (https://www.d-flight.it/new_portal/).

Geo-Zones are set up to:

- minimise safety risks
- protect the privacy of others
- address security issues
- deal with environmental concerns.

There are three main geo-zones for which Member States can adopt a colour coding to ensure airspace users can quickly identify what zone they refer to (tab. 4).

Table 4 - Classification of geo-zones based on drone flight permissions: excluded, restricted, and facilitated areas.

| | |
|---|---|
| | **Excluded geo-zones**<br><br>Flights are prohibited for operations in all or certain classes, hence **drone flying is not allowed.** |
| | **Restricted geo-zones**<br><br>UAS operations are limited and are subject to fulfilment of the set of conditions imposed in these zones. **You need prior authorisation to fly your drone** since you could be near areas such as airports, heliports, national parks, military installations, hospitals, nuclear power plants or any kind of key industrial site, etc. |
| | **Facilitated geo-zones**<br><br>UAS operations are facilitated in the 'Open' category, so **you can fly your drone.** |

### 4.2.2. Open category operations

Before each individual flight, the UAS operator must read laws regarding the use of airspace and the conformation of UAS geographical zones and check their area of operations on the maps on the d-flight portal. These maps show the "UAS geographical zones" provided for by art. 15 of Regulation (EU) 2019/947, which prohibits or limits flights in certain types of operations. These zones are divided into: zones established for "safety" reasons to protect airports, heliports, airfields/helipads; zones established for "security" reasons and zones for environmental protection reasons. The UAS geographical zones established for safety reasons are divided into sectors represented on d-flight with different colors: depending on the color, the geographical zone starts at a different height (e.g.: "red zone" 0 m, "orange zone" 25 m, etc.).

In UAS geographical zones established for safety reasons, the flight of UAS in the OPEN category is prohibited.
In some red zones, established for reasons other than safety, it is also possible to fly in the OPEN category, subject to a flight permit issued by the body/company that requested its establishment at the time.
To operate within these zones, it is first necessary to check whether there are additional limitations, such as, for example, that the flight with the UAS is linked to "aerial work" activities.
If it is not possible to fly in the OPEN category, operations must necessarily be conducted in the "SPECIFIC" category.

### 4.2.3. Operations in the SPECIFIC category (establishment of temporarily reserved or permanent zones) and derogation from the need for a clearance

Operations in the SPECIFIC category may be conducted according to standard scenarios (STS), or as reported in the Operational Authorization issued by Enac or in accordance with the LUC issued.
In the cases listed in paragraph 8.1 a), b) and c) of the Enac Circular ATM-09A, namely:
1. for operations within the geographical areas in the vicinity of airports (both civil and military);
2. if required by the risk assessment according to art. 11 of Regulation (EU) 2019/947;
3. for operations in the remaining airspace above the height of 120 m from the closest point to the earth's surface, the creation of an airspace reserve for UAS operations is required.
The UAS operator must obtain clearance to use the airspace. To obtain clearance it’s mandatory to ask the proper organization, depending on the state where you are operating.
Within the geographical areas in the vicinity of civil airports, the airspace reserve is not necessary if operating in the vicinity of artificial obstacles, namely:

- in the “red” zone, within a distance of 10 meters laterally and within 3 meters above the artificial obstacle, remaining more than 500 meters away from the airport grounds;
- in the zones of other colors, within a distance of 50 meters laterally and within 5 meters above the artificial obstacle.

In any case, the operator must receive permission from the owner of the obstacle. In the red zone the operation remains in the "SPECIFIC" Category, while in the zones of other colors the operation in the vicinity of the obstacle can also be conducted in the OPEN category.
N.B. The operator must first decide whether he can apply the standard scenario or whether it is necessary to submit an application to obtain an Operational Authorization. As part of this assessment, the additional need for a Flight Clearance emerges or not.
The clearance is required for carrying out a specific flight, if the limitations/conditions provided for in the Standard Scenario or in the Operational Authorization conflict with the conditions of the geographical areas reported on the d-flight portal for the area affected by the scheduled flight.
For operations within the UAS geographical zones in the vicinity of airports (point "1" above), if the flight does not take place within the airport grounds, the UAS operator may use, if applicable, the published standard scenarios. In this case, the clearance issued by the Territorial Directorate or the Air Force must satisfy the following conditions:
• it must be limited to the actual height at which the operations take place (which may be different from the one predefined in the specific standard scenario used);
• it must be retained by the operator and presented, in the event of checks, together with the declaration for standard scenarios ("declaration") previously made on the d-flight portal.
Limited to the airspaces in which air traffic control (ATC) services and the airport information service (AFIS) are provided, UAS operations for which an airspace reserve has been established are conducted in coordination with the ATS Unit responsible for the airspace concerned. An example of this are operations conducted within the airport ATZ.
In the case of UAS operations that require the continuous use of the areas (R), the UAS operator may be required to stipulate, with the responsible ATS unit, an Operations Letter which will report the methods of carrying out the operations in question and the specific responsibilities of the parties involved.

### 4.2.4. Specific category operations within the airport area

UAS operations on the airport area can only be conducted in the specific category – specific category, for needs related to airport activities, on civil airports and on military airports open to civil traffic (e.g. runway and infrastructure inspection, control of light systems and radio aids, aerial photogrammetric surveys, birdlife control, aircraft inspection, etc.). For this type

of operation, it is not possible to use STS scenarios, but the operational authorisation (Operational Authorisation) is required.

No airspace reservation or ATS assessment is required.

### 4.2.5. Overflight ban on natural parks and areas subject to wildlife protection

The Navigation Code, in art. 793, "Overflight bans", establishes that national organization that control the airspace "may prohibit overflight over certain areas of the national territory for reasons of safety or public order at the request of the competent administration".

Given the above, when requested by the park management body, the organization shall publish on the D-Flight platform any airspace restrictions for UAS operations.

In light of the above, overflight is prohibited only in those areas corresponding to the Parks whose ban has been approved by the organization and has therefore been published on the d-flight platform.

### 4.2.6. UAS operations on beaches during the bathing season

The organization that control the airspace in every nation, can prohibit overflights over certain areas of the national territory for safety reasons, as well as, upon request of the competent administration, in the presence of military reasons or reasons of security or public order.

With regard to UAS operations on beaches, the requirement that the remote pilot ensures that the UAS is kept at a sufficient safety distance from people and that it does not fly over crowds of people remains valid. With regard to the minimum safety distances to be maintained in open category operations, please refer to the following points of Regulation (EU) 2019/947:

1. for operations in subcategory A1: UAS.OPEN.020;
2. for operations in subcategory A2: UAS.OPEN.030;
3. for operations in subcategory A3: UAS.OPEN.040.

In order to ensure the safety, regularity and efficiency of UAS operations, in compliance with current international principles, all provisions for the disposition of national airspace are communicated to UAS operators through the d-flight application, and it is possible to prevent UAS activities, and sanction non-compliance with the ban, only when the relevant information is present on d-flight.

Finally, it should be noted that even if the rules relating to UAS operations are transposed, without alterations, into acts or provisions of non-aeronautical bodies, the competence relating to the imposition of sanctions remains with the organization.

## 4.3. Different type of sensors

### 4.3.1. Photogrammetric

The most common sensor is the Photogrammetric one, consisting of a high resolution camera (usually 12 MP or more). This sensor is used if the survey purpose is to have orthophotos and/or 3D models of the area object. The drone sellers usually provide a software to elaborate the images but many options are available, for example Agisoft Metashape. The Figure a side shows a DJI Mavic Enterprise 3E sensor.

### 4.3.2. LIDAR


With the new LIDAR sensor it is possible to simultaneously acquire pictures and LIDAR returns in order to have as a final product both a 3D model and a Digital Terrain Model. The new UAV developed sensors can read up to 5 laser returns allowing a high ground detection and good filtering of vegetation. The figure on the side shows a DJI Zenmuse L2 sensor.

### 4.3.3. Thermic

The thermic images have temperature information and can be used to detect water in buildings or in the grounds, cracks and hidden features not visible using normal sensors. The thermic survey provides additional information to the common survey. If the purpose is to build a thermal 3D model the suggestion is to increase the photo overlap because the thermic field of view is smaller than the Photogrammetric camera.

## 4.4. How to set up an acquisition

To perform a drone survey, 5 steps are necessary:

### 4.4.1. Identify the site

It's mandatory to check the site restrictions, it's possible to do this using a map service that shows the limitations for every site (https://www.easa.europa.eu/en/light/topics/geo-zones-know-where-fly-your-drone), D-Flight is the platform where are mapped all the restricted area (https://www.d-flight.it/new_portal/). Alternatively, it is possible to check on the map in the radio control.

### 4.4.2. Investigate the site

The Investigation part is a necessary step in order to detect the right place to take off, and the one with the best view of the area of interest. In this phase is necessary to evaluate whether other people are needed, particular attention must be paid to the topography; it is necessary to evaluate whether to use a DTM as a basis for the flight, especially in the case of steep terrain or terrain that changes morphology (hills, landslides, slopes that change inclination). In the following sections it will be explained how to prepare a correct DTM.

### 4.4.3. Set up Ground Control Points (GCPs), if necessary

This part consists in setting up the Ground Control Points or markers. The markers will be placed to the ground and will be georeferenced using a GPS station (Francioni et al., 2019). They will be used in the processing to georeference the pictures or the point cloud. The marker dimension must stand in the range 0.5x0.5 m to 1.5x1.5m, with a size less than 0.50 m it will be difficult to detect markers in the images. When the RTK positioning system (and module) is used during the flight, the number of GCPs necessary for georeferencing the models can be decreased or, when the area is not too wide, the use of GCPs could be not necessary .

### 4.4.4. Plan the flight mission

When all the necessary information are gathered it will be possible to plan the flight mission. The operator has to be sure to have the equipment ready: drone, battery, GCPs if is necessary, reserve battery, DTM (if is necessary). Check the weather forecast, there are many websites that give information for the drone flights, a good one, for example, is "oktofly" (https://oktofly.com/). It's mandatory to check the necessary documentation and if the area of interest is within a restricted zone and local drone regulations.

### 4.4.5. Execute the flight

In this phase it's necessary to have the maximum attention and be aware of all the dangers that can threaten the drone and the people. Flight always in line of sight, if you lost the drone pause the flight, and restart when you have the drone in your field of view. If something unexpected happens, pause the flight, if it's safe, land the drone, otherwise activate the return to home.

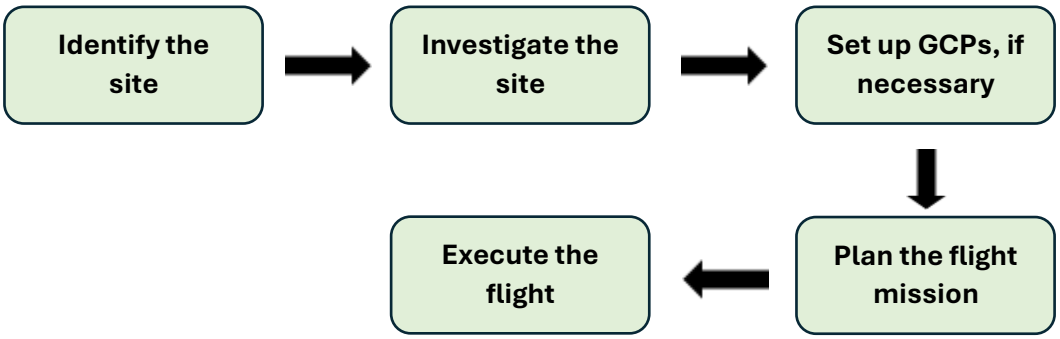


## 4.5. Data processing

In the data processing starting from the raw data it's possible to obtain a 3D Model, an Ortophoto and a DSM as final products. It's necessary to process the acquisition using a dedicated software, that can be Agisoft Metashape for Photogrammetry acquisition or DJI Terra for both Photogrammetry and LIDAR acquisitions. This manual does not cover how to process images but generally is a straight process with well determined steps.

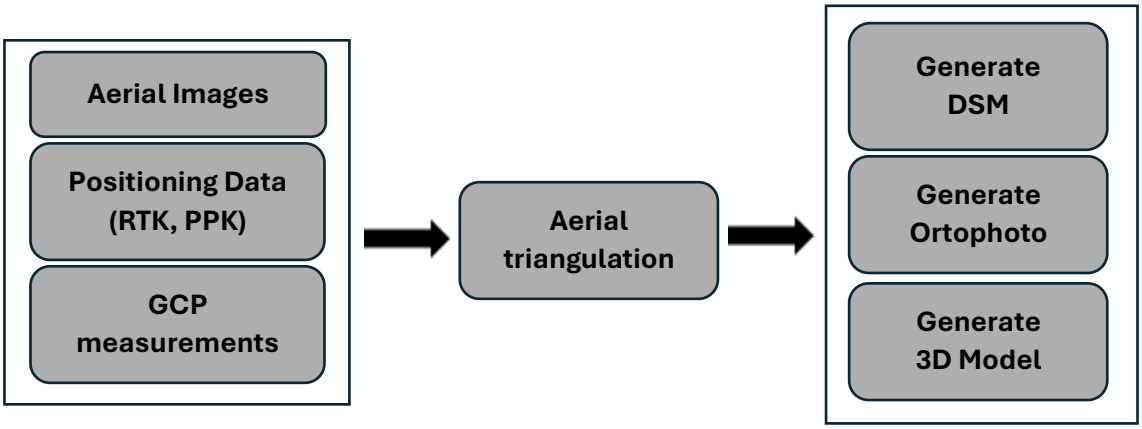

## 4.6. Digital Terrain Model (DTM) as a reference base

### 4.6.1. Why use a DTM

The use of a Digital Terrain Model (DTM) as a base for the survey is fundamental if the terrain is steep or presents features that emerge rapidly from the terrain, like a steep hill. In this scenario there are two main threats, first the drone can hit the ground, second there is the high possibility to collect data that does not overlap (Fig. 13). In this case the use of DTM as a base is strongly recommended.

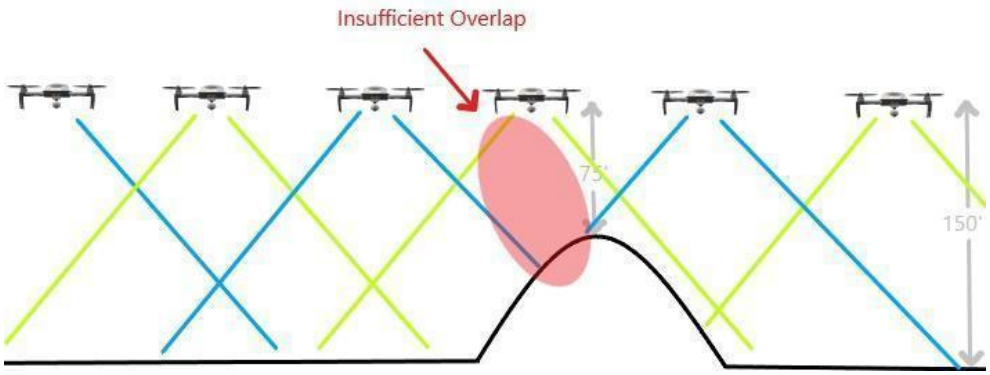


Figure 13 - Problems with steep ground features and overlapping.

### 4.6.2. DTM correction

The RTK positioning system used by the drone have ellipsoidal height while, usually, the available DTMs have geodetic height. It may be necessary, therefore, to correct the DTMs elevation information, so to match the quotes.

Hellipsoidic height can be added to the DTM using Python or Matlab, both codes are available at github repository https://github.com/ottaviani2/Drone_Survey_Guidelines.git.

## 4.7. Post Processing Kinematic (PPK)

Post-processing kinematic, often abbreviated as PPK, is a method used to improve the accuracy of positioning data collected through Global Navigation Satellite Systems (GNSS) when it is not possible to use RTK. In fact, unlike real-time methods RTK, PPK applies corrections to the collected data after the mission or survey is completed. This technique is

particularly useful in scenarios where real-time communication links are unreliable or unavailable, such as in remote areas or during drone flights (tab. 5).

In a typical PPK setup, there are two primary components: a moving GNSS receiver, referred to as the rover, and a stationary receiver, called the base station. Both devices independently record raw satellite data during the same period. Once the data collection is finished, the recorded information from both the rover and the base station is processed using specialized software. During this process, the system applies differential corrections to the rover's data using the more accurate, stable reference data from the base. The result is a significantly improved positional accuracy, often down to the centimeter level (tab. 5).

Table 5 - Comparison of PPK and RTK GNSS positioning methods in terms of timing, corrections, data link requirements, and accuracy.

| Feature | PPK | RTK |
|---|---|---|
| Timing | After data collection | In real time |
| Corrections | Applied post-mission | Applied during mission |
| Data link needed | No (only for download) | Yes (real-time link required) |
| Accuracy | High (cm-level possible) | Also high |

The post-processing itself is typically carried out using software solutions such as RTKLIB (an open-source tool), Emlid Studio, or commercial platforms from equipment manufacturers like Trimble, Leica, or Topcon. To perform PPK successfully, users need access to the raw GNSS data from both receivers, satellite ephemeris and clock data (which may be precise or broadcast), and relevant metadata including antenna positions and specifications.

While PPK adds an additional step after fieldwork, it offers a robust and accurate alternative to real-time solutions. It ensures that high-quality data can still be achieved even in challenging environments, making it a preferred method for many professionals who prioritize reliability and precision in GNSS-based positioning. To perform a PPK please follow

the steps indicated by DJI at this link (https://enterprise-insights.dji.com/blog/ppk-post-processed-kinematics-workflow).

## 4.8. Acquisition tips

### 4.8.1. Photogrammetric

If the purpose of the survey is to collect good pictures to realize a 3D model, the operator should be aware that the best weather condition is a cloudy sky that diffuses the light, deleting the shadows. In this specific condition the pictures have the best light available. A condition to strongly avoid is the one with long shadows in the ground, like early morning or close to the sunset, in those conditions the shadows move fast and can change position between two pictures, if the area is large. Those changings introduce an error and the software will be unable to correctly position the image. The suggested overlapping is 70-80% both forward and side. When the tophography is complex, it is suggested to use a DTM as base, so to acquire photographs from the same elevation.

### 4.8.2. LIDAR

LIDAR sensors are not sensitive to the light, but the same recommendations for the Photogrammetric acquisition are valid if the purpose of the survey is to collect pictures too. While performing a LIDAR acquisition it is necessary to evaluate the Gimbal inclination (sensor inclination). This depends on the amount of vegetation that is covering the area, the amount of battery that is available, and the steepness of the area. If the vegetation is dense, it is suggested to perform different acquisitions using different Gimbal inclination and flight direction. This allows to increase the final quality of the DTM (improving the filtering of vegetation) . The LIDAR per se doesn't need a strong side overlapping (20-30%), but if the acquisition has the purpose to collect pictures too, the suggested overlapping is 70-80% both forward and side.

### 4.8.3. Thermal Camera

If the purpose of the survey is only to acquire thermal photographs, there is no need to use high overlap. When the scope is to create 3D models, then the suggested overlapping is 70-80% both forward and side. The results of thermal surveys change within the day, in relation to the temperature and the exposition to sun rays.

Recent researches suggest that the best moment to carry surveys with thermal camera is after the sunset (in dark environmental conditions, so that parasite radiation was reduced to a minimum (Caliò et al., 2025). The effect of solar radiation, however, can persist even after the sunset, especially when an uneven slope heating by angulated sunrays occurred.

In conclusion, to fly a drone in a proper way, it is necessary to have a certification and to learn the laws that rule the matter of drones. It is necessary to be aware of the area where the drone flies, never over people, never over 120 meters from the ground. There are restricted areas, well documented at the portal D-Flight, where flight with drones may have restrictions. The five steps necessary to make a survey are: Identify the site, Investigate the site, Set up Ground Control Points (GCPs), Plan the flight mission, Execute the flight. Once the data are collected it is necessary to elaborate them using the right software.

Here some tips:

- if you are using LIDAR in a vegetated area make couple of different acquisition, if you have enough battery use inclined Gimbal;
- to modify the DTM height from geodetic to ellipsoidic you can use the code in this github repository (https://github.com/ottaviani2/Drone_Survey_Guidelines.git);
- if you don't have RTK available, you can use a GPS station to collect GPS data and associate them later to the acquisition using PPK.

# 5. HANDLE LIDAR SURVEY AND DATA ANALYSIS

This section outlines the procedures and equipment used for topographic data acquisition in coastal environments, with a focus on the use of handheld LiDAR scanning. The methodology is designed to ensure comprehensive spatial coverage, high-resolution point cloud generation, and efficient field operations in both open and complex terrains.

## 5.1. LiGrip 01 Lite RTK – Mobile LiDAR Scanner with GNSS Integration

The LiGrip 01 Lite RTK is a handheld mobile LiDAR system designed for high-precision outdoor topographic applications. It integrates a laser scanner with a real-time kinematic (RTK) GNSS module, enabling the real-time acquisition of georeferenced point clouds with centimeter-level accuracy. Additionally, it features an 8-megapixel camera that allows for true-color point cloud generation, enhancing the interpretability of the 3D model.

Its 70-meter scanning range and 200,000-point-per-second acquisition rate allow for the detailed reconstruction of complex landforms. The system is particularly well-suited for surveys conducted in open environments, such as dune systems or cliffed coasts, where the availability of GNSS signals is consistent and uninterrupted.

Main characteristics:

- Scanning range: up to 70 m
- Scan rate: 200,000 points/sec
- Positional accuracy: ±2 cm with RTK
- Camera: 8 MP for RGB point cloud coloring

Operational strengths:

- Enables high-resolution, georeferenced 3D mapping with real-time positional feedback.
- Effectively captures both horizontal terrain and vertical features such as escarpments or anthropogenic structures.
- Particularly advantageous in open terrain where GNSS positioning is stable and reliable.

## 5.2. Leica BLK2GO – Handheld LiDAR Scanner with SLAM Navigation

The Leica BLK2GO is a compact and highly portable handheld LiDAR scanner that employs a Simultaneous Localization and Mapping (SLAM) algorithm combined with inertial navigation (IMU) to estimate its position in space. It does not require GNSS signals to operate, navigation is performed via SLAM aided by the IMU, making it ideal for enclosed, vegetated, or architecturally complex environments where satellite reception is compromised or unavailable. (LiGrip can likewise operate in SLAM-only mode when GNSS is unavailable; RTK-GNSS is optional and used for direct georeferencing when satellites are available.

Despite its smaller size, the BLK2GO provides a high point acquisition rate of 420,000 points per second and integrates both a 12-megapixel high-resolution camera and three panoramic cameras for 360° contextual imaging. This setup facilitates the creation of visually enriched point clouds that aid in the interpretation and classification of the surveyed area.

Technical overview:

- Effective range: up to 25 m
- Scan rate: 420,000 points/sec
- Accuracy: ±1 cm
- Imaging: 12 MP main camera + three 4.8 MP panoramic cameras

Advantages in field conditions:

- Exceptional portability and ease of use in structurally or vegetatively complex environments.
- No onboard GNSS: operates purely on SLAM/IMU, enabling data collection in forested areas, under canopies, or within infrastructure. (LiGrip achieves the same in SLAM-only mode; RTK-GNSS is optional for direct georeferencing when available.)
- Real-time acquisition of both points clouds and photographic data, improving spatial awareness and facilitating post-processing.

## 5.3. Survey methodology and field protocols

The LiDAR surveys conducted with the LiGrip 01 Lite RTK and Leica BLK2GO followed standardized acquisition protocols aimed at ensuring high-quality, spatially consistent

datasets. While each instrument has unique features, a common methodological framework was established for calibration, data acquisition, and operator movement.

### 5.3.1. Initial Setup and Calibration

Prior to each survey, the scanner is connected to its dedicated mobile application (LiGrip App or BLK Live), which provides the operator with real-time visual feedback on scan coverage, device status, and operator path.

A standard calibration routine was followed to ensure positional accuracy:

- Reference Point Initialization - Every scan began and ended at the same physical location. This reference point is crucial for dataset alignment in post-processing and for maintaining spatial consistency across multiple acquisitions.
- IMU Calibration - The operator performed a figure-eight motion to initialize and stabilize the internal IMU system (Figure 14). This step is critical for devices that rely on inertial tracking (e.g., BLK2GO) and remains recommended for LiGrip, which also uses SLAM/IMU; it improves orientation accuracy and reduces drift, especially when operating without GNSS.

### 5.3.2. Structured Scanning Strategy

To ensure thorough surface coverage, a two-pass structured walk-through approach was implemented as shown in Figure 14:

- Forward Pass: The operator traversed the upper section of the beach, walking slowly while continuously rotating the scanner left and right to capture lateral and vertical features (e.g., cliffs, berms).
- Return Pass: A second scan was performed along the lower section of the beach, following a non-overlapping route. This ensured coverage of underrepresented surfaces and increased point cloud density.

This dual-path strategy is particularly effective in complex coastal settings where surface geometry varies dramatically and occlusions are common. It also allows the entire survey to be conducted by a single operator, increasing operational efficiency.

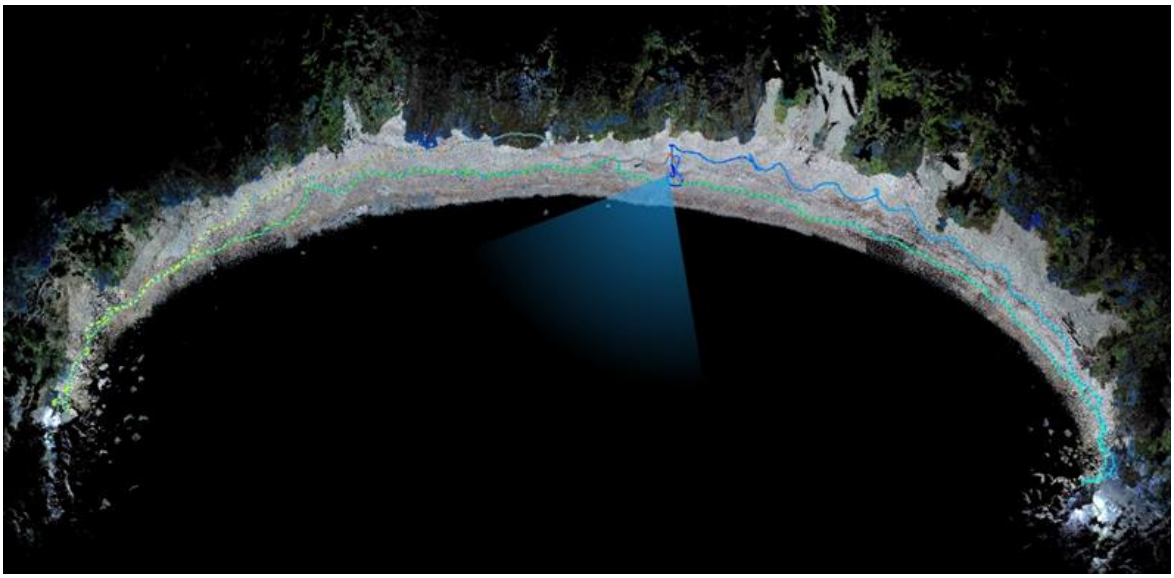

Figure 14 - Two pass structure walk and calibration

## 5.4. Instrument performance: advantages and limitations

### 5.4.1. LiGrip 01 Lite RTK – SLAM Scanner with Optional RTK-GNSS

Advantages:

- High Accuracy: Real-time RTK corrections ensure centimeter-level positional accuracy across large, open areas.
- Colorized Output: The integrated camera allows generation of georeferenced point clouds in true color.
- Field Efficiency: A single operator can conduct surveys with minimal setup time.

Limitations:

- Direct georeferencing depends on GNSS availability: in enclosed or obstructed areas the device operates in SLAM-only mode (scanning is unaffected), but global accuracy can drift over long, feature-poor segments.
- Can operate without GNSS using SLAM; when RTK corrections are available, data are directly georeferenced to a global coordinate system.
- Weight and Portability: Bulkier than the BLK2GO, which can affect operator endurance

over long distances or rugged terrain.

- Water Surface Limitations: As with most terrestrial LiDAR systems, laser beams reflect off water surfaces, making it unsuitable for capturing submerged features.
- Mitigation Measures:
- Ground control points (GCPs) were placed strategically to support post-processing georeferencing in GNSS-challenged environments.

### 5.4.2. Leica BLK2GO – SLAM-Based Scanner

Advantages:

- Full Mobility: Lightweight and ergonomic, ideal for confined or vegetated environments.
- Integrated Imaging: Simultaneous capture of high-resolution photographs enhances the interpretability of point cloud data.
- Rapid Data Collection: Enables quick scanning with minimal logistical preparation.

Limitations:

- No GNSS/RTK Integration: Relies exclusively on SLAM and IMU tracking, which can drift over long, feature-poor areas.
- Shorter Range: Limited to a maximum of 25 meters, making it less suitable for very large or tall structures.
- Calibration Requirement: Initial figure-eight motion is essential for accurate inertial tracking; improper execution can degrade scan accuracy.

## 5.5. Integration of UAV and LIDAR systems

The combination of UAV photogrammetry and handheld LiDAR scanning offers a complementary and highly effective survey solution, particularly in coastal and geomorphologically complex environments.

Benefits of Integration:

- Extended Coverage: UAV imagery complements terrestrial scanning by covering submerged zones and large horizontal surfaces not accessible by ground-based systems.
- Enhanced Accuracy: The fusion of RTK-GNSS data (e.g., from LiGrip), SLAM technology, and photogrammetric outputs ensures a detailed, georeferenced, and accurate 3D representation of the terrain and structures.

- Vertical and Oblique Geometry Capture: Handheld scanners excel in capturing undercut features, cliffs, and vertical surfaces that are often problematic for aerial-only methods.

## 6. REFERENCES


- Aizebeokhai, A. P., Olayinka, A. I., & Singh, V. S. (2010). Application of 2D and 3D geoelectrical resistivity imaging for engineering site investigation in a crystalline basement terrain, Southwestern Nigeria. Environmental Earth Sciences, 61, 1481. https://doi.org/10.1007/s12665-010-0474-z
- Amidu, S. A., & Olayinka, A. I. (2006). Environmental assessment of sewage disposal systems using 2D electrical resistivity imaging and geochemical analysis: A case study from Ibadan, Southwestern Nigeria. Environmental and Engineering Geoscience, 7(3), 261–272.
- Caliò, D., Intelisano, M., Pappalardo, G., & Mineo, S. (2025). Infrared thermal dense point clouds: A new frontier for remote landslide investigation. ISPRS Journal of Photogrammetry and Remote Sensing, 224, 155–165. https://doi.org/10.1016/j.isprsjprs.2025.04.003
- Dahlin, T., & Loke, M. H. (1997). Quasi-3D resistivity imaging – Mapping of three-dimensional structures using two-dimensional DC resistivity techniques. In Proceedings of the 3rd Meeting of the Environmental and Engineering Geophysical Society, 143–146.
- Deere, D. U., Hendron, A. J., Patton, F., & Cording, E. J. (1967). Design of surface and near surface excavations in rock. In C. Fairhurst (Ed.), Proceedings of the 8th U.S. Symposium on Rock Mechanics: Failure and Breakage of Rock (pp. 237–302). AIME, New York.
- Francioni, M., Simone, M., Stead, D., Sciarra, N., Mataloni, G., & Calamita, F. (2019). A new fast and low-cost photogrammetry method for the engineering characterization of rock slopes. Remote Sensing, 11(11). https://doi.org/10.3390/rs11111267
- Griffiths, D. H., Turnbull, J., & Olayinka, A. I. (1990). Two-dimensional resistivity mapping with a complex controlled array. First Break, 8, 121–129.
- Hoek, E., & Bray, J. W. (1981). Rock Slope Engineering (3rd ed.). Institution of Mining and Metallurgy.

- ISRM (1978). Suggested methods for the quantitative description of discontinuities in rock masses. International Journal of Rock Mechanics and Mining Sciences & Geomechanics Abstracts, 15, 319–368.
- Leucci, G. (2006). Contribution of ground-penetrating radar and electrical resistivity tomography to identify the cavity and fractures under the main church in Botrugno (Lecce, Italy). Journal of Archaeological Science, 33(9), 1194–1204. https://doi.org/10.1016/j.jas.2005.12.009
- Leucci, G. (2007). Geoscientific investigations for mapping the subsidence risk in an urban area. Journal of Geophysics and Engineering, 4, 317–331. https://doi.org/10.1088/1742-2132/4/3/S11
- Leucci, G. (2019). Nondestructive Testing for Archaeology and Cultural Heritage: A Practical Guide and New Perspective. Springer. ISBN 978-3-030-01898-6.
- Leucci, G. (2020). Advances in Geophysical Methods Applied to Forensic Investigations: New Developments in Acquisition and Data Analysis Methodologies. Springer. ISBN 978-3-030-46241-3.
- Leucci, G., De Giorgi, L., & Gizzi, F. T., Persico, R. (2017). Integrated geo-scientific surveys in the historical centre of Mesagne (Brindisi, Southern Italy). Natural Hazards, 86, 363–383. https://doi.org/10.1007/s11069-016-2645-x
- Leucci, G., De Giorgi, L., & Scardozzi, G. (2014). Geophysical prospecting and remote sensing for the study of the San Rossore area in Pisa (Tuscany, Italy). Journal of Archaeological Science, 52, 256–276. https://doi.org/10.1016/j.jas.2014.08.028
- Loke, M. H., Chambers, J. E., Rucker, D. F., Kuras, O., & Wilkinson, P. B. (2013). Recent developments in the direct-current geoelectrical imaging method. Journal of Applied Geophysics, 95, 135–156. https://doi.org/10.1016/j.jappgeo.2013.02.017
- Negri, S., Leucci, G., & Mazzone, F. (2008). High-resolution 3D ERT to help GPR data interpretation for researching archaeological items in a geologically complex subsurface. Journal of Applied Geophysics, 65(3–4), 111–120. https://doi.org/10.1016/j.jappgeo.2008.06.004
- Palmström, A. (1982). The volumetric joint count – A useful and simple measure of the degree of rock jointing. Proceedings of the 4th International Congress of the International Association for Engineering Geology, Delhi, 5, 221–228.

- Palmström, A., & Lien, R. (1985). Handbook of Engineering Geology Rock.
- Palmstrom, A., & Broch, E. (2006). Use and misuse of rock mass classification systems with reference to the Q-system. Tunnelling and Underground Space Technology, 21, 575–593.
- Palmstrom, A., & Singh, R. (2001). The deformation modulus of rock masses: Comparisons between in situ tests and indirect estimates. Tunnelling and Underground Space Technology, 16, 115–131.
- Reynolds, J. M. (2011). An Introduction to Applied and Environmental Geophysics (2nd ed.). Wiley-Blackwell, Oxford. p. 696.
- Sarma, V. S. (2014). Electrical resistivity (ER), self-potential (SP), induced polarisation (IP), spectral induced polarisation (SIP) and electrical resistivity tomography (ERT) prospection in NGRI for the past 50 years. Journal of the Indian Geophysical Union, 18(2), 245–272.
- Sen, Z., & Eissa, E. A. (1991). Volumetric rock quality designation. Journal of Geotechnical Engineering, 117(9), 1331–1346.
- Sen, Z., & Eissa, E. A. (1992). Rock quality charts for log-normally distributed block sizes. International Journal of Rock Mechanics and Mining Sciences.
- Terzaghi, K. (1946). Introduction to tunnel geology. In: Rock Tunnelling with Steel Supports, by Proctor and White, pp. 5–153.